Patterns in Mie scattering: evolution when normalized by the Rayleigh cross section

Matthew J. Berg, Christopher M. Sorensen, and Amit Chakrabarti

An alternative to using the traditional scattering angle θ to describe light scattering from a uniform dielectric sphere is the dimensionless parameter qR, where R is the radius of the sphere, $q = 2k \sin(\theta/2)$, and k is the wavenumber of the incident light. Simple patterns appear in the scattered intensity if qR is used in place of θ. These patterns are characterized by the envelopes approximating the scattered intensity distributions and are quantified by the phase-shift parameter $\rho = 2kR|m - 1|$, where m is the real refractive index of the sphere. Here we find new patterns in these envelopes when the scattered intensity is normalized to the Rayleigh differential cross section. Mie scattering is found to be similar to Rayleigh scattering when $\rho < 1$ and follows simple patterns for $\rho > 1$, which evolve predictably as a function of ρ. These patterns allow us to present a unifying picture of the evolution of Mie scattering for changes in kR and m.

OCIS codes: 290.0290, 290.4020.

1. Introduction

Light scattering is an important unintrusive tool for studying the size, shape, structure, and composition of particles and particle systems.[1] It is also important for determining the effects of aerosol particles in the atmospheric environment and is the basis of many naturally occurring optical phenomena.[1] Many particle systems contain spherical particles, and spherical particles are frequently used for modeling more complex systems.[1] The formal solution of Maxwell's equations for the interaction of a uniform dielectric sphere with a time harmonic electromagnetic field (light scattering) was achieved by Mie in 1908.[2] From Mie theory the scattered fields can be calculated for any location inside or outside a sphere. The explicit mathematical solution is often expressed as an expansion of the scattered field in electric and magnetic partial waves.[3] Consequently, the general Mie solution can be complex and inaccessible to simple physical interpretation on the basis of its mathematical form alone.

Previous work from this laboratory has uncovered a number of simple patterns in Mie scattering.[4–6] In particular, when the scattered intensity is plotted as a function of the scattering wave vector [see Eq. (1) in Subsection 2.B] rather than the scattering angle, universal features that are amenable to physical interpretation are seen.[4] Following this work Xu and Alfano described the same patterns in very large spheres using the geometrical optics approximation.[7] Also, Jonsson *et al.* showed that the simple functionality discussed in Ref. 4 persists in multiple-scattering calculations.[8]

Here we extend the work of Ref. 4 to both incident polarizations, and uncover and describe unique patterns. We conclude with a general description of light scattering from spheres of arbitrary size and real refractive index.

2. Mie Scattering Curves

A. Scattering Geometry

Our considerations in this work are restricted to the scattering of light from a homogeneous dielectric sphere of radius R situated in an external homogeneous dielectric medium. The quotient of the refractive index of the sphere to the refractive index of the external medium defines a relative index m, and we limit ourselves to nonabsorping and nonmagnetic refractive indices. The sphere is centered at the coordinate origin, and the incident light is taken to be a monochromatic electromagnetic plane wave traveling in the positive z direction (see Fig. 1). The point external to the sphere, where we are

The authors are with the Department of Physics, Kansas State University, Manhattan, Kansas 66506. C. M. Sorensen's e-mail address is sor@phys.ksu.edu.

Received 3 March 2005; accepted 4 April 2005.
0003-6935/05/347487-07$15.00/0

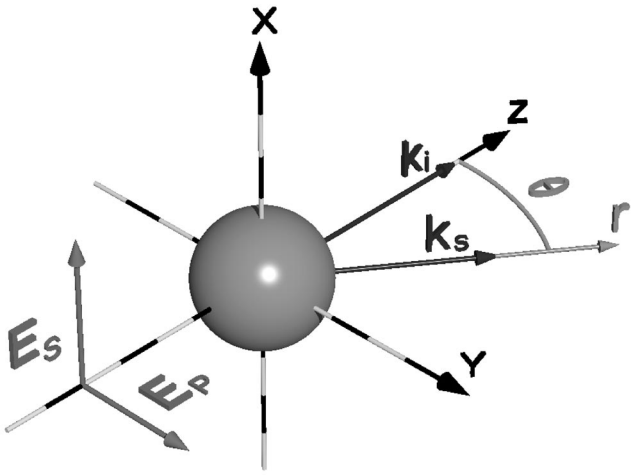

Fig. 1. Coordinate geometry used for calculating the scattering of light from a homogeneous nonmagnetic dielectric sphere. The S and P polarizations of the incident electric field are shown with respect to the scattering plane.

interested in the electromagnetic field intensity, is located by $\mathbf{r}$.

The propagation of the incident light is given by the wave vector $\mathbf{k_i}$, where $|\mathbf{k_i}| = 2\pi/\lambda$ and λ is the wavelength of the incident light in the external medium. With $\mathbf{r}$ we can define the scattered wave vector $\mathbf{k_s}$, which gives the direction of propagation of the scattered light and points along $\mathbf{r}$. We take the magnitudes of the incident and scattered wave vectors to be equal, $|\mathbf{k_i}| = |\mathbf{k_s}| = k$, meaning that the incident light is scattered elastically. Together $\mathbf{k_i}$ and $\mathbf{k_s}$ define the scattering plane. The angle between $\mathbf{k_i}$ and $\mathbf{k_s}$ is the scattering angle θ. The polarization of the incident light is defined relative to the scattering plane and is assumed to be either perpendicular or parallel to the plane. If the incident light is polarized perpendicular to the scattering plane, then the scattered light at $\mathbf{r}$ (with $\mathbf{r}$ confined to the scattering plane) will also be polarized perpendicular to the scattering plane.[2] We refer to this configuration as S polarization. Similarly, if the incident light is polarized parallel to the scattering plane, then the scattered light will be polarized the same. We refer to this configuration as P polarization.

B. Background: Patterns Discovered in Our Previous Work

In many one-dimensional light-scattering situations, the scattered light intensity is measured as a function of the scattering angle θ. Often the functional form of this intensity versus scattering angle data is complicated, making interpretation difficult. Previous work by Sorensen and Fischbach showed that distinct patterns appear when the scattered intensity is plotted as a function of the scattering wave vector $\mathbf{q}$ in place of the scattering angle θ.[4] The scattering wave vector is the difference between the incident and scattered wave vectors, $\mathbf{q} = \mathbf{k_s} - \mathbf{k_i}$, and since we only consider elastic scattering the magnitude of $\mathbf{q}$ is

$$q = 2k \sin\left(\frac{\theta}{2}\right). \tag{1}$$

The representation of scattered intensity as a function of $\mathbf{q}$ is referred to in this work as "q-space analysis."

Sorensen and Fischbach use an adaptation of the BHMIE algorithm developed by Bohren and Huffman.[9] The BHMIE algorithm produces the scattered Mie differential cross section normalized in the forward direction to the intensity of light incident on the sphere. For brevity, we refer to the normalized Mie differential cross section as simply the Mie scattered intensity, I.

When I as a function of the dimensionless variable qR is plotted in a log–log plot, the intensity curves are found to be bounded by three linear envelopes. The linearity of the envelopes implies an overall power-law dependence of I on qR, even though the scattered intensity distribution also shows a complex structure of interference maxima and minima, called the ripples. In effect, the bounding envelopes serve as a coarse average of the detailed interference structure. The envelopes show a semiquantitative universality parameterized by the phase-shift parameter

$$\rho = 2kR|m - 1|. \tag{2}$$

The patterns in these envelopes can be summarized as follows:

$$I \propto (qR)^0 \text{ for } 0 < qR < 1, \tag{3a}$$

$$I \propto (qR)^{-2} \text{ for } 1 < qR \lesssim \rho \text{ if } \rho > 1, \tag{3b}$$

$$I \propto (qR)^{-4} \text{ for } qR \gtrsim \rho. \tag{3c}$$

The $\rho \to 0$ and small kR limit is the Rayleigh scattering limit with a cross section given by

$$\frac{d\sigma}{d\Omega_{\text{Ray}}} = k^{-2}(kR)^6\left(\frac{m^2 - 1}{m^2 + 2}\right)^2. \tag{4}$$

Rayleigh scattering is isotropic in the scattering plane for S-polarized light, i.e., it has no θ, hence no q dependence. For P-polarized incident light an additional dipole factor of $\cos^2(\theta)$ is included in Eq. (4). Because Eq. (3a) is isotropic, we call Eq. (3a) the "Rayleigh regime" of forward scattering present in scattering by all particles.

In the limit that $\rho \to 0$ but arbitrary kR, the Mie solution simplifies to the Rayleigh–Debye–Gans (RDG) differential cross section, which is

$$\frac{d\sigma}{d\Omega_{\text{RDG}}} = \frac{d\sigma}{d\Omega_{\text{Ray}}}\left[\frac{3\sin(qR) - 3qR\cos(qR)}{(qR)^3}\right]^2. \tag{5}$$

The RDG cross section follows Eqs. (3a) and (3c) but not (3b) since $\rho < 1$. Sorensen and Fischbach showed that the Mie patterns evolve from the $\rho \to 0$ limit of Eq. (5) to Eqs. (3a)–(3c) with increasing ρ.

3. New Patterns

A. Smoothing by Averaging over Sphere Sizes

To further investigate the patterns present in Mie scattering, we average the scattered intensity for a distribution of sphere radii. This averaging is done to smooth out the ripples, revealing the general structure of the intensity curves. We could alternatively look at the envelopes bounding the intensity curves, but work by Mishchenko *et al.* shows that using a size distribution to average the scattered intensity provides a straightforward way to reveal the general structure of the scattering curves.[1] We use a logarithmic normal distribution, which gives a weight value $w(R)$,

$$w(R) = \exp\left\{-\frac{1}{2}\left[\frac{\ln(R/R_m)}{\ln(\sigma)}\right]^2\right\}. \tag{6}$$

This radii distribution is controlled by two parameters: the most probable sphere radius R_m and the logarithmic geometric mean standard deviation σ (labeled as LGMSD in the figures). The value of σ determines the width of the distribution and provides a measure of the averaging affect on the intensity. To remove the ripples in the Mie curves, the size distribution in Eq. (6) is integrated over R with the Mie scattering intensities. The value of σ is increased until the ripples essentially disappear, but is increased no further to avoid eliminating any larger features of the scattering structure. We find that a value of $\sigma = 1.22$ does this the best. In the following considerations where this size distribution is used, all the parameters characterizing the scattering process, which involve the sphere radius (e.g., kR, ρ), are calculated using R_m but designated with R, e.g., kR_m is designated as kR. Application of radii distribution smoothing to the RDG cross section when normalized by the Rayleigh cross section yields $(9/2)(qR)^{-4}$ for large qR.

B. Similarities between Mie and Rayleigh Scattering

In Figs. 2(a) and 3(a) the Mie scattered intensity per unit incident intensity is shown as a function of qR for spheres of two different m. The bold curves represent scattering of S-polarized light, whereas the dotted curves represent scattering of P-polarized light. There are several features to notice in these plots:

(i) The overall scattering increases rapidly with kR.

(ii) For $qR \lesssim 1$, a flat, slope-equal-to-zero, forward-scattering Rayleigh regime occurs in all the plots that correspond to Eq. (3a). For large kR the forward scattering is independent of m.

(iii) For $qR > 1$ the plots fall off quickly, the functionality of which will be described below.

(iv) A complex backscattering, the glory, develops near $qR \approx 2kR$. We have been unable to find any describable patterns in the glory.

(v) The difference between S and P polarization is less for large kR and large m. For small kR there is a minimum in the P polarization near $qR = \sqrt{2}kR$ corresponding to $\theta = 90°$. This is consistent with the limit $kR = 0$ of a dipole scattering pattern.

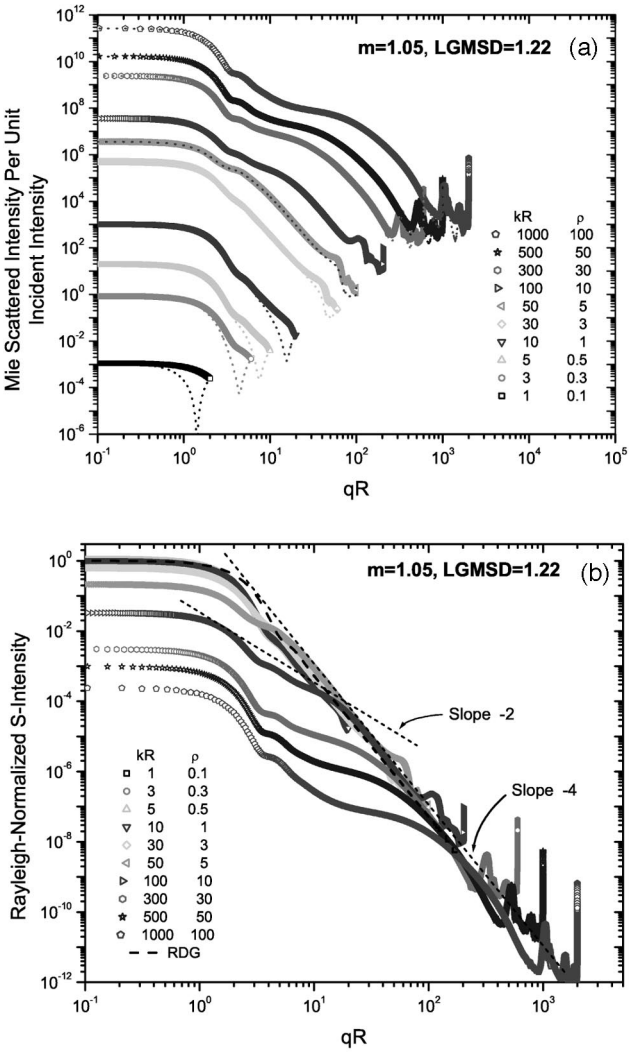

Fig. 2. (a) Mie scattered intensity normalized to the intensity of the incident light. The scattered intensity is plotted as a function of qR for spheres with $m = 1.05$ and various kR. The bold curves represent scattering of incident S-polarized light and the dotted curves represent scattering of P-polarized light. (b) S-polarized Mie scattered intensity normalized by the Rayleigh differential cross section for the same spheres as in (a). The averaged RDG envelope is shown as the bold dashed curve and the $(qR)^{-2}$ and $(qR)^{-4}$ envelopes are shown as thin dashes for the $kR = 100$ curve. For clarity, the legends in both figures show the data sets in the same order as they appear in the figure. For example, the top curve in (a) corresponds to the top entry in the legend, $kR = 1000$.

To see the similarities between the Mie and Rayleigh cross sections and to further explore the manner in which the Mie curves evolve away from the Rayleigh limit, we normalize the Mie curves by the Ray-

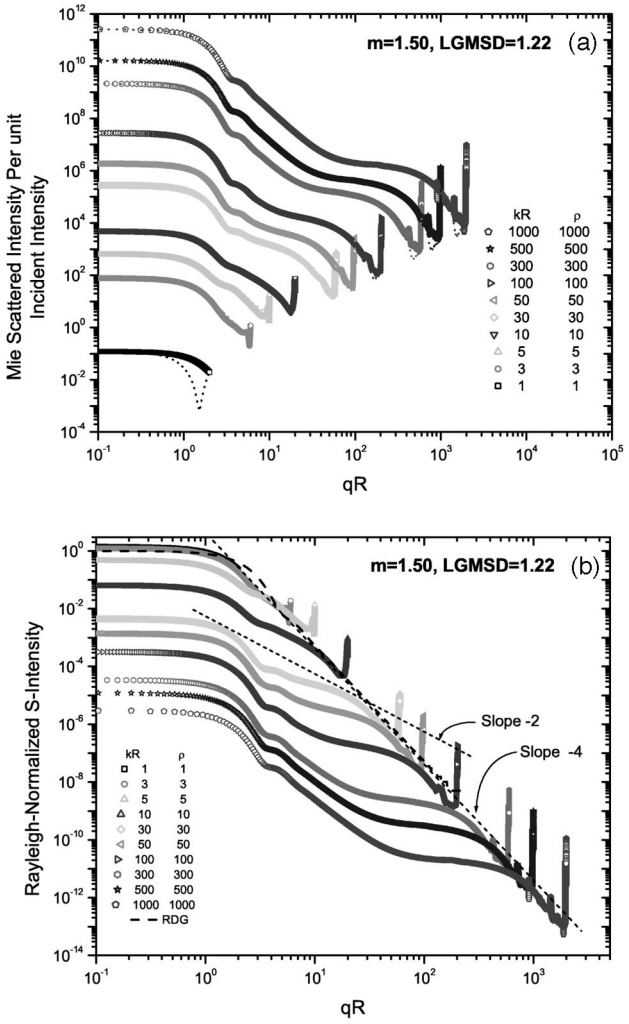

Fig. 3. (a) Mie scattered intensity normalized to the intensity of the incident light. The scattered intensity is plotted as a function of qR for spheres with $m = 1.50$ and various kR. The bold curves represent scattering of incident S-polarized light and the dotted curves represent scattering of P-polarized light. (b) S-polarized Mie scattered intensity normalized by the Rayleigh differential cross section for the same spheres as in (a). The averaged RDG envelope is shown as the bold dashed curve and the $(qR)^{-2}$ and $(qR)^{-4}$ envelopes are shown as thin dashes for the $kR = 30$ curve. For clarity, the legends in both figures show the data sets in the same order as they appear in the figure. For example, the top curve in (a) corresponds to the top entry in the legend, $kR = 1000$.

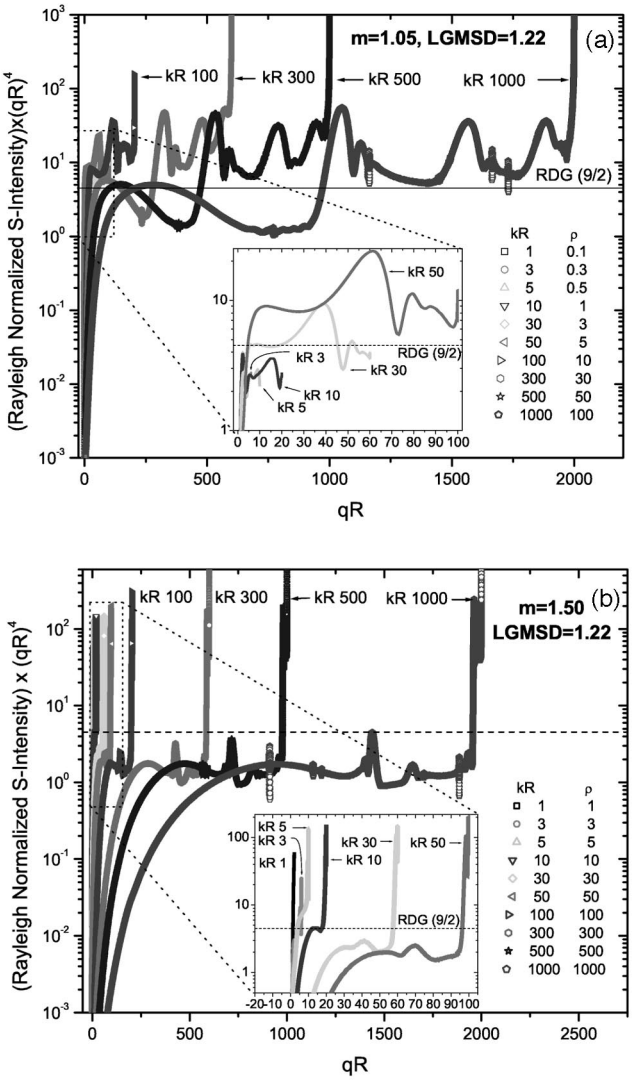

Fig. 4. Rayleigh-normalized Mie intensity multiplied by $(qR)^4$ for spheres of (a) $m = 1.05$ and (b) $m = 1.50$, and for various kR values. Shown as dashes in both plots is the averaged RDG limit of 9/2.

leigh cross section given by Eq. (4). To evaluate Eq. (4) for the same optical properties as the spheres with which we wish to compare, we must assign a value for the wavelength of incident light. This wavelength is arbitrary for our purposes and is taken to be $\lambda = 200\pi$ nm.

Plots of the Mie scattered intensity normalized by the Rayleigh cross section, a quantity we will call the "Rayleigh-normalized scattered intensity," are shown in Figs. 2(b) and 3(b) [the same data in Figs. 2(a) and 3(a), respectively.] There are several features to notice in these plots:

(i) For $\rho < 1$ the curves fall on top of each other. They display the $(qR)^0$ and $(qR)^{-4}$ regimes of Eqs. (3a) and (3c). For all kR at large qR the $(qR)^{-4}$ regime is consistent with the RDG limit.

(ii) As ρ increases beyond 1, the curves begin to separate and shift down from the $\rho < 1$ curves for $qR \lesssim \rho$. Hence Mie scattering is smaller than the Rayleigh prediction. Then an approximate $(qR)^{-2}$ regime develops between $qR \approx 1$ and $qR \approx \rho$. In general, the curves sag below $(qR)^{-2}$ between these limits, which are well connected by $(qR)^{-2}$.

(iii) For $qR > \rho$ *all* curves are bounded by the *same* $(qR)^{-4}$ envelope (if the glory spikes are ignored).

To study the large qR regime in more detail, Figs. 4(a) and 4(b) show the Rayleigh-normalized intensity multiplied by $(qR)^4$. Here any dependence of the averaged scattered intensity on $(qR)^{-4}$ is seen as a flat, zero slope trend in the curves. The plots also show the averaged RDG limit of 9/2. Excluding the glory,

we see that the Mie curves for $m = 1.05$ in Fig. 4(a) follow $(qR)^{-4}$ but with variations with a total spread of roughly an order of magnitude. The RDG limit of 9/2 is roughly in the geometric middle of this variation. For $kR < 30$ the variation is always below the RDG 9/2 limit. Figure 4(b) shows that for $m = 1.50$ the $(qR)^{-4}$ again applies on average and displays variations of approximately half of an order of magnitude. Unlike the $m = 1.05$ data, all curves for $kR > 10$ fluctuate below the RDG 9/2 limit.

These results remind us that the envelopes that we describe as bounding the Mie curves are only intended to represent the general features of the intensity distributions. In this coarse analysis we neglect factors of the order of 3 separating the envelopes from the actual Mie intensity distributions. Of course we have already ignored the complex, fine-structured interference ripples.

C. Forward Scattering

Figures 2(b) and 3(b) show that intensity in the forward-scattering Rayleigh regime, $qR < 1$, becomes less than the Rayleigh value when $\rho > 1$. To investigate this further we plot in Fig. 5(a) the Mie forward-scattered intensity in the limit $\theta \to 0$ normalized to the Rayleigh differential cross section as a function of ρ for spheres of different m. Figure 5(a) shows that the Rayleigh-normalized forward scattering falls off roughly as ρ^{-2} for $\rho > 1$. Exploring this in more detail, we plot in Fig. 5(b) the Rayleigh-normalized, forward-scattering multiplied by ρ^2. We summarize the patterns in Figs. 5(a) and 5(b) with the following features:

(i) All spheres with $\rho \lesssim 1$ scatter in the forward direction with the same intensity as the Rayleigh differential cross section, which is consistent with the $\rho < 1$ behavior seen in Figs. 2(b) and 3(b).

(ii) For $\rho > 1$, the curves for different m begin to separate and oscillate. Near $\rho \approx 2$–3, the forward scattering exceeds the Rayleigh scattering by nearly a factor of 3 for large m. For $\rho > 5$ the oscillations decay and a $c\rho^{-2}$ functionality develops, where c is a constant of the order of $\sqrt{10}$ unique to a given m.

(iii) The oscillatory structures of the curves are in phase with each other and the oscillations increase in amplitude with m but eventually die away at large ρ.

D. Total Cross Section

It is known that as kR increases beyond 1, spheres scatter the majority of incident light in the forward direction.[2] If forward scattering is dominant, then we expect a connection between the patterns in forward scattering and the total Mie scattered cross section σ_{Mie}. Figure 6 shows σ_{Mie} as a function of kR for spheres with different m. We find that:

(i) The total cross section σ_{Mie} for spheres with $\rho < 1$ is the same as the total Rayleigh cross section $\sigma_{\mathrm{Ray}} = (8\pi/3)(d\sigma/d\Omega_{\mathrm{Ray}})$. Curves of different m in the $kR < 1$ range show a clear m dependence, which is explained by the m functionality in Eq. (4).

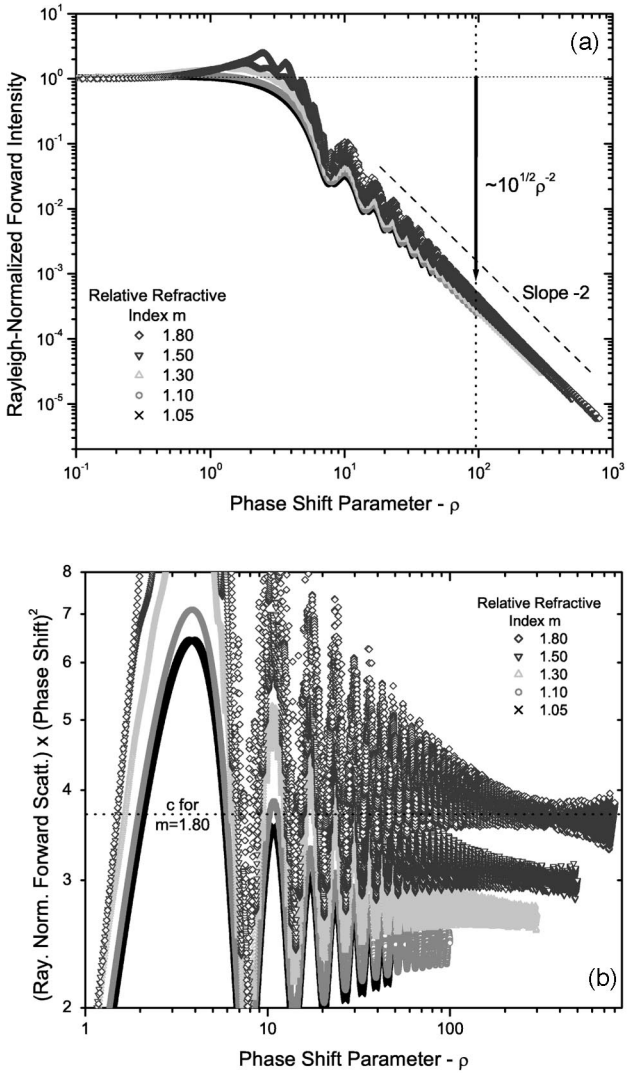

Fig. 5. (a) Mie forward-scattered intensity normalized by the Rayleigh differential cross section for spheres of various m. The -2 slope is shown to illustrate the $c\rho^{-2}$ evolution of the curves. (b) Rayleigh-normalized forward scattering multiplied by ρ^2. For clarity, both legends show the data sets in the same order as they appear.

(ii) As R grows to values for which $\rho > 2$, the R^6 dependence crosses over, through a ripple structure, to a geometric R^2 (i.e., the geometric cross section of the sphere) dependence at large ρ. The separation between curves of different m in the Rayleigh regime begins to vanish.

(iii) As R continues to increase, all curves converge onto a value of twice the geometric cross section of the sphere with no m dependence, and the ripple structure decays away.

(iv) For $kR \gg 1$, σ_{Mie} is approximately equal to $(\sigma_{Ray})/(c^2\rho^4)$, where $c^2 \approx 10$.

4. Discussion and Conclusion

We have seen that unique patterns in the light-scattering properties of spheres appear if the scattered intensity is normalized in q space by the

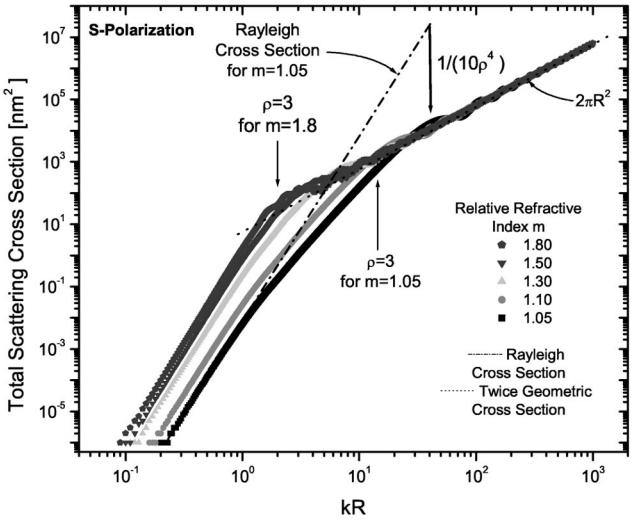

Fig. 6. Total Mie cross section σ_{Mie} for various m and incident light with S polarization and $\lambda = 200\pi$ nm. The large ρ behavior of $\sigma_{Mie} \approx 2\pi R^2$ is shown as the dotted curve. σ_{Ray} is shown as the long dashed line for $m = 1.05$. The vertical arrow shows the factor $1/(c^2\rho^4)$, where $c \approx \sqrt{10}$, relating σ_{Ray} to σ_{Mie}, for $m = 1.05$, in the $\rho > 1$ range. For clarity, the legend shows the data sets in the same order as they appear in the figure.

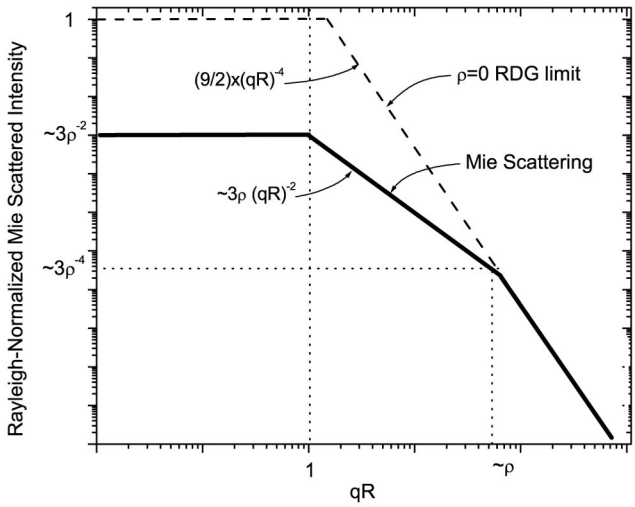

Fig. 8. Diagram of the averaged Rayleigh-normalized Mie scattering patterns for nonmagnetic uniform spheres of arbitrary size and real refractive index parameterized by $\rho = 2kR|m - 1| > 1$ (thick solid curve). In this example $\rho \approx 55$. The thin dashed curve is the RDG limit, $\rho \to 0$.

Rayleigh differential cross section. A consequence of Rayleigh normalization is that it allows us to see that the scattered intensity curves for different values of ρ evolve in an orderly way. The evolution of the curves is controlled exclusively by the phase-shift parameter ρ, which affords us a simple picture of how Mie scattering changes with the size and optical properties of the sphere.

Figure 7 demonstrates the evolution of the Rayleigh-normalized Mie scattering intensity. Many of the features described above are contained in this figure. Figure 7 also illustrates the quasi-universality of Mie scattering on the phase-shift parameter ρ, described by Sorensen and Fischbach. For each phase-shift parameter value shown the values of m and kR vary widely. Despite this variation, the curves for the same ρ lie with each other, hence the curves are universal with ρ. This universality is not perfect, however, with variations of approximately a factor of 3 for the same ρ. Hence we use the term "quasi-universal" to describe the ρ functionality.

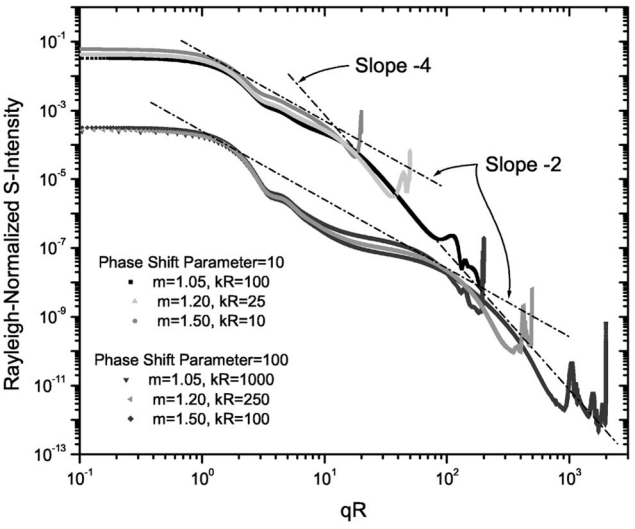

Fig. 7. Two sets of Rayleigh-normalized Mie intensity curves. The three curves in each set have the same value of ρ but different values of kR and m. The bounding envelopes are shown for both sets of curves and illustrate how the envelopes only depend on ρ.

Figure 8 gives a general description of light scattering from a sphere of arbitrary size and real refractive index; it includes the Rayleigh, RDG, and Mie limits. We see in Fig. 8 that the Mie scattering patterns start at $\rho = 0$ with the RDG limit. For $qR < 1$ the RDG curve is flat, i.e., $(qR)^0$ and equivalent to Rayleigh scattering. For $qR > 1$ it falls off with a negative four power law, the Porod limit, with magnitude $(9/2)(qR)^{-4}$ times the Rayleigh scattering cross section. Note that this includes Rayleigh scattering in the limit $\lambda \gg R$ because then $qR \ll 1$ and only the flat part of the scattering function is obtained.

When $\rho > 1$, scattering in the Rayleigh regime decreases relative to true Rayleigh scattering. The relative decrease (remember, the nonnormalized scattering increases with ρ) is proportional to ρ^2 as depicted in Fig. 8. For $qR > 1$ the scattering now falls off as $(qR)^{-2}$ until this functionality crosses the RDG curve at $qR = \rho$. For $qR > \rho$ the scattering is identical to RDG scattering, falling off as $(qR)^{-4}$ for all R and m as long as $qR > \rho$. The $(qR)^{-2}$ functionality between $qR = 1$ and ρ for $\rho > 1$ is exact only at those limits. The average Mie curves dip below the $(qR)^{-2}$ line. This dip is the first interference minimum present in all Mie curves and is the strongest of all the minima. Its position is near $qR \approx 3.5$.

The patterns in Mie scattering can be useful in practice to estimate quantities of interest in situations involving single scattering from uniform dielectric spherical particles. For example, if the light intensity scattered from a spherical particle of unknown dimension is measured and plotted log–log as a function of q, the radius of the sphere may be estimated from the q value at which the intensity distribution envelopes change from a slope of zero to a slope of -2 or -4 [see Eqs. (3a) and (3b)]. Additionally, the simplicity of the Mie patterns and the intuition that they engender allow one, in the laboratory or the field, to estimate the magnitude and angular distribution of scattering without resorting to complex calculations.

We acknowledge the support of NASA Graduate Student Research Program grant NNG04GL59H, NASA grant NAG3-2360, and National Science Foundation grant CTS-0080017.

References

1. M. I. Mishchenko, L. D. Travis, and A. A. Lacis, *Scattering, Absorption, and Emission of Light by Small Particles* (Cambridge U. Press, 2002).
2. M. Born and E. Wolf, *Principles of Optics* (Cambridge U. Press, 1999).
3. M. Kerker, *The Scattering of Light and Other Electromagnetic Radiation* (Academic, 1969).
4. C. M. Sorensen and D. J. Fischbach, "Patterns in Mie scattering," Opt. Commun. **173,** 145–153 (2000).
5. C. M. Sorensen and D. Shi, "Guinier analysis for homogeneous dielectric spheres of arbitrary size," Opt. Commun. **178,** 31–36 (2000).
6. C. M. Sorensen and D. Shi, "Patterns in the ripple structure of Mie scattering," J. Opt. Soc. Am. A **19,** 122–125 (2002).
7. M. Xu and R. R. Alfano, "More on patterns in Mie scattering," Opt. Commun. **226,** 1–5 (2003).
8. J. C. Jonsson, G. B. Smith, and G. A. Niklasson, "Experimental and Monte Carlo analysis of isotropic multiple Mie scattering," Opt. Commun. **240,** 9–175 (2004).
9. C. F. Bohren and D. R. Huffman, *Absorption and Scattering of Light by Small Particles* (Wiley, 1983).